



Calhoun: The NPS Institutional Archive
DSpace Repository

Faculty and Researchers

Faculty and Researchers Collection

2008

An evaluation of microstructure and
microhardness in copper subjected to
ultra-high strains

Zhilyaev, A.P.

Springer

A.P. Zhilyaev, S. Swaminathan, A.A. Gimazov, T.R. McNelley, T.G. Langdon, "An evaluation of microstructure and microhardness in copper subjected to ultra-high strains," *Journal of Materials Science*, v. 43, (2008), pp. 7451-7456.

<http://hdl.handle.net/10945/55874>

Downloaded from NPS Archive: Calhoun



Calhoun is a project of the Dudley Knox Library at NPS, furthering the precepts and goals of open government and government transparency. All information contained herein has been approved for release by the NPS Public Affairs Officer.

Dudley Knox Library / Naval Postgraduate School
411 Dyer Road / 1 University Circle
Monterey, California USA 93943

<http://www.nps.edu/library>

An evaluation of microstructure and microhardness in copper subjected to ultra-high strains

A. P. Zhilyaev · S. Swaminathan · A. A. Gimazov ·
T. R. McNelley · T. G. Langdon

Received: 28 February 2008 / Accepted: 6 May 2008 / Published online: 13 July 2008
© Springer Science+Business Media, LLC 2008

Abstract The microstructure and microhardness of copper subjected to large strains either using one or a combination of severe plastic deformation (SPD) processing techniques was evaluated. The individual SPD techniques used include equal-channel angular pressing (ECAP), high-pressure torsion (HPT), and chip formation during machining (M). Microstructural characterization using orientation imaging microscopy provided detailed information on the grain sizes and misorientation statistics after different processing routes. Vickers indentation analysis was used to evaluate the hardness of the deformed samples. The results show that excellent microstructures and properties are achieved when these three processes are used in combination, including grain sizes in the range of ~ 0.2 – 0.3 μm and hardness values up to $>1,900$ MPa.

A. P. Zhilyaev (✉)

Department of Physical Metallurgy, Centro Nacional de Investigaciones Metalúrgicas, CSIC, 28040 Madrid, Spain
e-mail: AlexZ@anrb.ru

A. P. Zhilyaev · A. A. Gimazov

Institute for Metals Superplasticity Problems, RAS, 450001 Ufa, Russia

S. Swaminathan · T. R. McNelley

Department of Mechanical & Astronautical Engineering,
Naval Postgraduate School, 700 Dyer Road, Monterey,
CA 93943-5146, USA

T. G. Langdon

Departments of Aerospace & Mechanical Engineering
and Materials Science, University of Southern California,
Los Angeles, CA 90089-1453, USA

T. G. Langdon

Materials Research Group, School of Engineering Sciences,
University of Southampton, Southampton SO17 1BJ, UK

Introduction

The application of large strain deformation, using techniques such as equal-channel angular pressing (ECAP) [1, 2], high-pressure torsion (HPT) [3, 4], and chip formation in plane-strain machining (M) [5, 6] have demonstrated that bulk materials with nanocrystalline microstructures may be produced in a wide variety of metals and alloys at near-ambient temperatures. Systematic studies of the microstructural refinement achieved using processes of severe plastic deformation (SPD) have shown that dislocation multiplication and interaction dominate at low strains and this leads to the formation of elongated nanocrystalline structures as the imposed strain increases. Upon further straining, these elongated structures transform into essentially equiaxed nanocrystalline structures. The formation of equiaxed nanocrystalline structures occurs concurrently with an increase in the fraction of high-angle grain boundaries having misorientation angles of $>15^\circ$.

Despite the significant differences in the strain paths leading to grain refinement in the various individual SPD processing methods, the final equilibrium microstructure of a material subjected to large strains is always reasonably equiaxed in nature with the grains having almost dislocation-free interiors. This has led to a major effort that has been focused on adjusting the processing and material conditions to attain equilibrium equiaxed microstructures using the most expeditious processing procedure. For example, processing by route B_C in ECAP, in which the billets are rotated about their longitudinal axes by 90° in the same sense between each pass [7], is now established as producing equiaxed nanocrystalline structures by grain subdivision at the fastest rate in metals and dilute alloys [8].

It is envisaged that critical engineering components having high strength nanocrystalline microstructures may be produced by SPD techniques. Therefore, it is crucial to understand the thermal and stress-induced stability of these structures during service, because the large fraction of high-angle boundaries may provide an impetus for grain growth. The thermal stability of nanocrystalline materials was studied in several earlier investigations [9–13], but in contrast, the stress-induced stability has received only limited attention.

It is difficult to interpret the tensile stress–strain behavior of these equiaxed nanocrystalline microstructures because the severe strain hardening leads to an early onset of plastic instability [14]. Nevertheless, it is reasonable to anticipate that a continued intense deformation of the nanocrystalline microstructures may provide some insight into the stress-induced stability of these materials. Furthermore, parallel work on selected electro-deposited materials such as copper, where the grains sizes are ~30–40 nm and therefore an order of magnitude smaller than in many SPD materials, has shown that grain growth occurs under a complex compressive stress state produced by indentation [15]. Accordingly, the objective of the present work was to analyze the stability of the nanocrystalline microstructures produced by SPD techniques when the materials are subjected to ultra-high strains under high quasi-hydrostatic compressive stresses. These compressive stresses were achieved by subjecting samples to a combination of various SPD techniques.

Experimental material and procedures

The copper material used in this study had a purity of 99.9% and an initial grain size of 500 μm . The copper was subjected to ECAP processing by route B_C to four passes at room temperature using a 90° die having a zero relief angle at the outer die channel intersection; the ideal shear strain imposed during this processing was 8. Constrained HPT was performed on the initial copper samples for a total of $N = 5$ turns under an applied pressure P of 6 GPa. The consolidated HPT samples were 10-mm diameter discs with a thickness (t) of 0.2 to 0.3 mm. The shear strain introduced in the HPT samples varied with radius R of the disk according to $10\pi R/t$ [4]. Large shear strains ~10 were also introduced into the initial copper material by chip formation during machining (M) operation by milling. The chips were machined at a rate of 30 m min⁻¹ using a -5° rake angle tool. TEM observations indicated that the microstructure of copper after being subjected to large strains by each of the above-mentioned processes was made up of equiaxed nanostructured grains. The microstructure after HPT was made up of 320-nm grains,

whereas the microstructure in the flow plane of copper after ECAP processing was made up of equiaxed nanocrystalline structures having sizes of 500 nm [16]. In this study, the microstructure of the milled chips was not obtained directly but was inferred from another study where copper was subjected to nearly equivalent machining conditions and showed a grain size of ~300 nm [6]. In order to understand the compressive stress behavior of these equiaxed nanocrystalline microstructures, the ECAP samples and machining chips were placed in the depression on the lower anvil of a constrained HPT facility and consolidated at room temperature under the same conditions as that used for the initial copper material. Further, the chips were milled from the ECAP samples using the same machining parameters and these chips, in turn, were also subjected to HPT at $P = 6\text{GPa}$ and $N = 5$ turns.

Microstructure analysis was performed using transmission electron microscopy (TEM) and orientation imaging microscopy (OIM). Samples of ultrafine-grained copper were metallographically polished followed by electropolishing using a solution of 85 vol% H₃PO₄ in water at 20 °C with a voltage of 15 V. The OIM was conducted in a TOPCON S-510 scanning electron microscope operating at 15 kV with a LaB₆ filament having a step-size of 0.05 μm . The OIM study involved standard clean-up procedures [17, 18]: (i) grain dilatation with a grain tolerance angle (GTA) of 5°; a minimum grain size (MGS) of two pixels; (ii) grain confidence index (CI) standardization with GTA = 5° and MGS = 2°; and (iii) neighbor CI correlation with minimum CI of 0.05. The mechanical properties of the consolidated discs were also characterized using Vickers indentation. The discs were polished to a mirror-like finish and tested using a load of 100 g with a holding time of 10 s. The average hardness was determined from five separate measurements.

Results and discussion

Figure 1 shows representative inverse pole figure maps of copper after the following processing routes: (a) subjected to HPT from the initial material, (b) after M followed by HPT, (c) after ECAP followed by HPT, and (d) after ECAP followed by M and then HPT. The microstructures in all conditions were equiaxed with measured average grain sizes of 0.26, 0.24, 0.27, and 0.22 μm , respectively, where full details are given in Table 1. The grain sizes measured from OIM were similar to the grain sizes reported from TEM observations [16]. Indeed, a comparison between Figs. 1a and 2 taken from the earlier report [16] shows a similarity in both the appearance of the microstructure and the grain size. In the OIM images as in Fig. 1a, there was some evidence for twinning, as indicated by the small oval,

Fig. 1 Grain boundary maps of UFG copper after (a) HPT, (b) M + HPT, (c) ECAP + HPT, and (d) ECAP + M + HPT

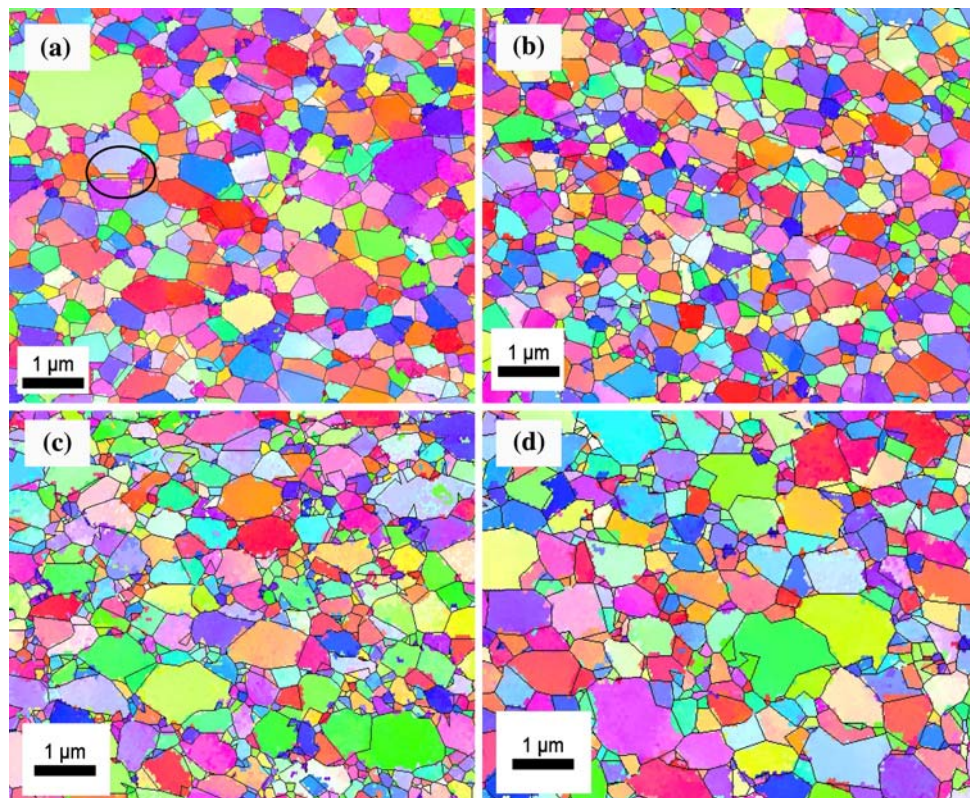


Table 1 Grain size and grain boundary statistics by OIM

| Specimen | Mean grain size (μm) | | GB statistics | | |
|----------------|----------------------|------|---------------|------|------------|
| | TEM [12] | OIM | HAB | LAB | CSL (Σ3) |
| HPT | 0.32 | 0.26 | 0.58 | 0.32 | 0.10 (2.7) |
| M + HPT | 0.31 | 0.24 | 0.69 | 0.19 | 0.12 (3.3) |
| ECAP + HPT | 0.31 | 0.27 | 0.51 | 0.35 | 0.14 (3.9) |
| ECAP + M + HPT | 0.21 | 0.22 | 0.62 | 0.25 | 0.13 (3.5) |

The area-weighted average grain size (D_{AW}) was obtained from OIM studies and converted to mean linear intercept value (D_{MLI}) by the relation: $D_{AW} \approx 1.728 D_{MLI}$ [22]

and this is similar to the twin which is clearly visible in the TEM microstructure in Fig. 2.

Using OIM measurements, the maximum grain sizes observed in copper samples after different types of large strain deformation are documented in Table 2 together with details of the relative fractions of the various grain sizes in increments of 20%. It is apparent that a large fraction of grains lies within 0–20% of the maximum grain size for all processing conditions and this is consistent with the average grain sizes reported in Table 1. Processing by HPT gave the largest grains as is evident in the upper left corner of Fig. 1a, although these unusually large grains were not present after combinations of other SPD processes. Table 1 also lists the relative fraction of high-angle boundaries (HAB) where the orientations are $>15^\circ$, the fraction of low-angle boundaries



Fig. 2 TEM microstructure of HPT copper [16]

(LAB), and the fraction of CSL ($\Sigma 3$) boundaries. These statistics show that the fraction of high-angle boundaries in the equiaxed nanocrystalline grains is $>60\%$ in all samples. Also, the relative fraction of CSL boundaries, including the fraction of $\Sigma 3$ boundaries, remains the same even when copper is subjected to larger strains.

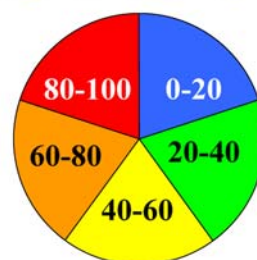
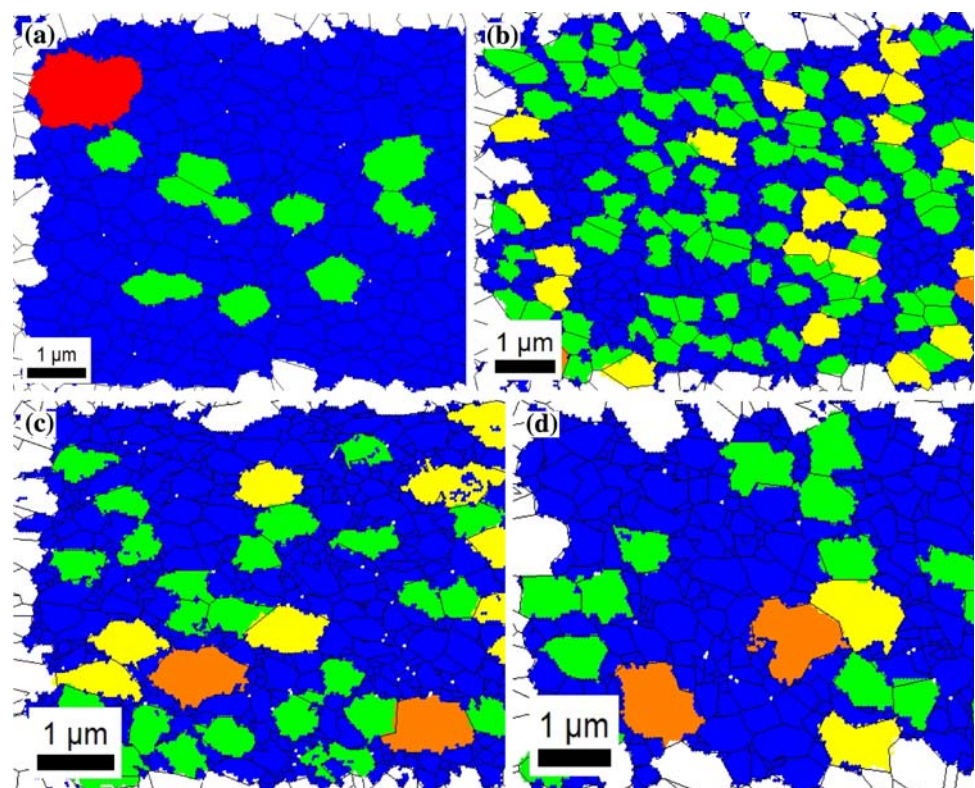
Table 2 Spatial distribution of grains in relation to maximum observed grain size

| Specimen | Maximum grain size (μm) | Fraction (%) | | | | |
|----------------|--------------------------------------|--------------|-------|-------|-------|--------|
| | | 0–20 | 20–40 | 40–60 | 60–80 | 80–100 |
| HPT | 1.40 | 0.89 | 0.08 | 0 | 0 | 0.03 |
| M + HPT | 0.85 | 0.57 | 0.27 | 0.11 | 0.04 | 0.01 |
| ECAP + HPT | 0.98 | 0.72 | 0.18 | 0.07 | 0.02 | 0.01 |
| ECAP + M + HPT | 0.98 | 0.77 | 0.15 | 0.03 | 0.02 | 0.03 |

Figure 3 displays the same grain topological map as in Fig. 1 but with the microstructure presented in a different format so that the grains within selected size ranges are highlighted: this display is based on the information in Table 2, where the ranges of grain sizes are presented as percentages of the maximum grain size. Thus, the alternative displays in Fig. 3 reflect the morphological differences in the microstructures of all specimens examined in this investigation. For example, in the case of

copper processed only by HPT and shown in Fig. 3a, there is a relatively homogeneous matrix with small inclusions of larger grains and a single isolated larger grain within the area covered by the OIM scanning. For the chips consolidated by HPT in Fig. 3b, there is a more homogeneous microstructure. Finally, for combinations of ECAP + HPT and ECAP + M + HPT shown in Fig. 3c and d, there is a higher fraction of large grains, as shown in Table 2, but nevertheless these large grains are smaller than the isolated

Fig. 3 Grain distribution maps of copper after (a) HPT, (b) M + HPT, (c) ECAP + HPT, and (d) ECAP + M + HPT



large grain observed in copper processed only by HPT in Fig. 3a. Figure 3 therefore provides a very clear morphological description of the differences between these various microstructures.

Inspection showed that the microtexture of samples subjected to large strains exhibited mixtures of recrystallization and almost complete shear textures. For example, a microtexture analysis of the ECAP + M + HPT sample revealed a cube recrystallization texture in addition to an B-fiber shear texture, as shown in Fig. 4.

Hardness measurements were performed after subjecting copper to large strains by these various SPD techniques, either separately or in combination, and the results are plotted in Fig. 5. For the various techniques taken in isolation, the highest hardness is attained after HPT, which is consistent with earlier experiments showing that HPT gives the smallest grain size [19]. In general, however, the average value of the hardness increases on imposition of large strains by combining different techniques. The highest hardness of 1,940 MPa in the present investigation was observed for copper subjected to the three separate processes of ECAP + M + HPT. An additional important observation is that the hardness indentations showed no visible signs of cracking under the optical microscope even in the samples subjected to ECAP + M + HPT. This demonstrates that, despite the very large strain imposed through the use of a combination of SPD techniques, copper has the capability of withstanding the complex

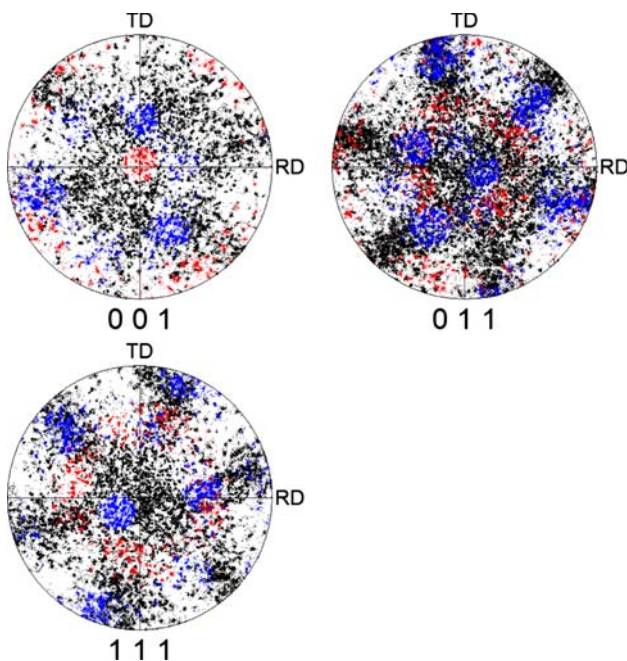


Fig. 4 Rotated to the flow plane pole figure of ECAP + M + HPT sample showing the presence of recrystallized grains (cube-texture in red) and deformed grains (B-type shear texture in blue)

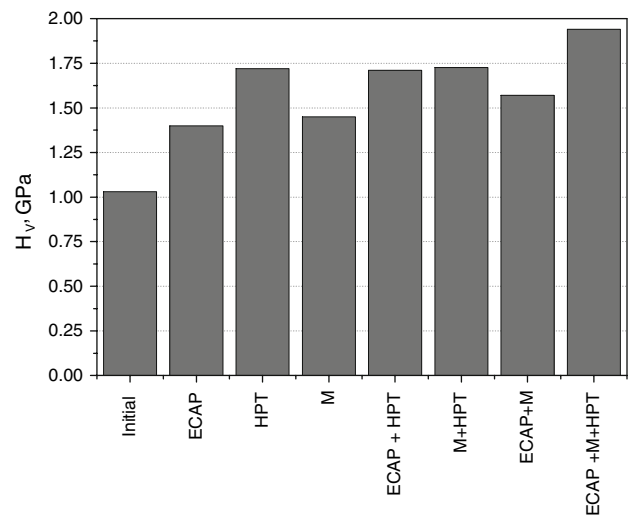


Fig. 5 Vickers microhardness of copper subjected to different deformation histories

compressive stresses that are an inherent feature of the indentations.

From this analysis, it is evident that the equiaxed nanocrystalline structures formed in copper after SPD processing show excellent stability even under the application of ultra-high plastic strains. The average grain size of the nanocrystalline structures decreased as the strain level was increased through the use of multiple SPD processes, and this decrease led to a concomitant increase in hardness, as shown in Fig. 5. The copper subjected to machining and HPT contained the highest fraction of high-angle boundaries of ~69%, but there was no evidence of any run-away grain growth in this sample or in any of the other samples subjected to multiple SPD processing. This result therefore confirms recent experimental data for commercial purity aluminum [20] and pure nickel [21], where HPT straining was continued for 20 whole revolutions.

The presence of concurrent deformation and adiabatic heating leads to copper samples having a mixture of deformation and recrystallization textures after multiple SPD processing. In earlier studies, the dislocation density after multiple SPD processing was shown to be higher than the density recorded after a single SPD process [16, 21]. Furthermore, samples of an Al–7% Si alloy were shown earlier to experience an estimated temperature rise of up to ~120 °C in HPT processing [22]. This estimated rise is in very good agreement with experimental measurements on commercial purity aluminum showing the occurrence of a temperature rise of ~50 °C at a distance of 1 mm from the contact between the upper anvil and the disk during HPT, especially when it is noted that there is an anticipated steep temperature gradient within the HPT facility. Based on these measurements, it is reasonable to assume that the

temperature rise in copper may be even higher than in aluminum, and thus, it may reach the recrystallization temperature of ~ 150 °C during SPD processing by HPT [23]. However, it appears that concurrent deformation by HPT stabilizes the equiaxed nanocrystalline microstructures even in samples experiencing large prior strains by ECAP and M. A similar conclusion was reached in another recent investigation, which examined the influence of the relaxation processes on structure formation in pure metals and alloys during HPT and led to the conclusion that processing of copper gave dynamically recrystallized grains [24].

The results from this investigation suggest the potential for using SPD processing for the production of materials for use as engineering components, where the service conditions entail high compressive stresses. Thus, it appears feasible to use this approach in the production of meso-scale components requiring a reasonable level of wear resistance.

Summary and conclusions

1. The SPD processing of copper by various methods leads to the formation of essentially equiaxed nanocrystalline structures.
2. This equiaxed structure is relatively stable even under the application of compressive stresses and adiabatic heating. In addition, these equiaxed nanocrystalline structures exhibit an increase in hardness under application of further compressive stresses.
3. The results show that excellent properties and microstructures are attained by using combinations of equal-channel angular pressing, machining, and high-pressure torsion.
4. The evidence suggests that SPD processing may be useful for the production of materials for use as engineering components experiencing compressive stress states in service.

Acknowledgements One of the authors (APZ) thanks the Spanish Ministry of Education and Science (under the Ramón y Cajal program) for financial support. Another author (TGL) was supported by the National Science Foundation of the United States under Grant No. DMR-0243331.

References

1. Segal VM, Reznikov VI, Drobyshvskiy AE, Kopylov VI (1981) *Russ Metall* 1:99
2. Valiev RZ, Langdon TG (2006) *Prog Mater Sci* 51:881. doi:10.1016/j.pmatsci.2006.02.003
3. Zhilyaev AP, Lee S, Nurislamova GV, Valiev RZ, Langdon TG (2001) *Scripta Mater* 44:2753. doi:10.1016/S1359-6462(01)00955-1
4. Zhilyaev AP, Nurislamova GV, Kim B-K, Baró MD, Szpunar JA, Langdon TG (2003) *Acta Mater* 51:753. doi:10.1016/S1359-6454(02)00466-4
5. Swaminathan S, Brown TL, Chandrasekar S, McNelley TR, Compton WD (2007) *Scripta Mater* 56:1047. doi:10.1016/j.scriptamat.2007.02.034
6. Swaminathan S, Ravi Shankar M, Rao BC, Compton WD, Chandrasekar S, King AH, Trumble KP (2007) *J Mater Sci* 42:1529. doi:10.1007/s10853-006-0745-9
7. Furukawa M, Iwahashi Y, Horita Z, Nemoto M, Langdon TG (1998) *Mater Sci Eng A* 257:328. doi:10.1016/S0921-5093(98)00750-3
8. Oh-ishi K, Horita Z, Furukawa M, Nemoto M, Langdon TG (1998) *Metall Mater Trans* 29A:2011. doi:10.1007/s11661-998-0027-z
9. Wang J, Iwahashi Y, Horita Z, Furukawa M, Nemoto M, Valiev RZ, Langdon TG (1996) *Acta Mater* 44:2973. doi:10.1016/1359-6454(95)00395-9
10. Furukawa M, Iwahashi Y, Horita Z, Nemoto M, Tsenev NK, Valiev RZ, Langdon TG (1997) *Acta Mater* 45:4751. doi:10.1016/S1359-6454(97)00120-1
11. Ferrasse S, Segal VM, Hartwig KT, Goforth RE (1997) *Metall Mater Trans* 28A:1047. doi:10.1007/s11661-997-0234-z
12. Hasegawa H, Komura S, Utsunomiya A, Horita Z, Furukawa M, Nemoto M, Langdon TG (1999) *Mater Sci Eng A* 265:188. doi:10.1016/S0921-5093(98)01136-8
13. Neishi K, Horita Z, Langdon TG (2002) *Mater Sci Eng A* 325:54. doi:10.1016/S0921-5093(01)01404-6
14. Dalla Torre F, Lapovok R, Sandlin J, Thomson PF, Davies CHJ, Pereloma EV (2004) *Acta Mater* 52:4819. doi:10.1016/j.actamat.2004.06.040
15. Brandstetter S, Zhang K, Escudero A, Weertman JR, Van Swygenhoven H (2008) *Scripta Mater* 58:61. doi:10.1016/j.scriptamat.2007.08.042
16. Zhilyaev AP, Gimazov AA, Raab GI, Langdon TG (2008) *Mater Sci Eng A* 486:123
17. OIM user's manual, EDAX-TSL, E. Mahway, NJ, 2005
18. Zhilyaev AP, Oh-ishi K, Raab GI, McNelley TR (2006) *Ultrafine grained materials IV*. In: Zhu YT, Langdon TG, Horita Z, Zehetbauer MJ, Semiatin SL, Lowe TC (eds) *The Minerals, Metals and Materials society*, Warrendale, PA, p 113
19. Dutkiewicz J, Kuśnierz J, Maziarz W, Lejkowska M, Garbacz H, Lewandowska M, Dobromyslova AV, Kurzydowski KJ (2005) *Phys Stat Sol (a)* 202:2309. doi:10.1002/pssa.200521235
20. Todaka Y, Umamoto M, Yamazaki A, Sasaki J, Tsuchiya K (2008) *Mater Trans* 49:7. doi:10.2320/matertrans.ME200713
21. Zhilyaev AP, Gimazov AA, Soshnikova EP, Révész Á, Langdon TG (2008) *Mater Sci Eng A* 489:207
22. Zhilyaev AP, Garcia-Infanta JM, Carreno F, Langdon TG, Ruano OA (2007) *Scripta Mater* 57:763. doi:10.1016/j.scriptamat.2007.06.029
23. Jiang H, Zhu YT, Butt DP, Alexandrov IV, Lowe TC (2000) *Mater Sci Eng A* 290:128. doi:10.1016/S0921-5093(00)00919-9
24. Degtyarev MV, Chashchukhina TI, Voronova LM, Patselov AM, Pilyugin VP (2007) *Acta Mater* 55:6039. doi:10.1016/j.actamat.2007.04.017